Flux tubes in $U(1)$ Lattice Gauge Theory

André da Conceição Amado
Under supervision of Pedro José de Almeida Bicudo
Dep. Physics, IST, Lisbon, Portugal

November 29, 2012

Abstract

In this work we implement a numerical code to study several aspects of $U(1)$ Lattice Gauge Theory, mainly properties of confining phase.

We start with a general introduction to the subject of Lattice Gauge Theory.

We utilize Polyakov loop correlations to study $4D$ compact $U(1)$ flux tubes and the static electron-positron potential in lattice gauge theory. By using field operators we are able to probe directly the electric and magnetic fields. Also we study the evolution of the potential with β as well as other already well-known quantities. In order to improve the signal-to-noise ratio in the confinement phase, we apply the Lüscher-Weiss multilevel algorithm.

We study a range of temperatures from 0.05 T_c to 0.40 T_c and our results follow the Effective String Theory prediction for the relation between the the static charge distance and the width of the tube flux in the whole range. We are able to observe the transition from logarithmic to linear behavior.

Our code is completely written in CUDA, and we run it in NVIDIA FERMI generation GPU's, in order to achieve the necessary performance for our computations.

Keywords: Lattice Gauge Theory, $U(1)$, flux tubes, Lattice QCD, static potential, Effective String Theory

1 Introduction

Lattice Quantum Field Theory (LQFT) is an area of study increasingly important in Quantum Field Theory. The recent important advances, both theoretical and of computational capacity, open new horizons of study and allow this theory to reach areas it could not before.

LQFT opens the possibility of a better understanding of confining mechanisms an area of study closed to the usage of perturbative tools.

In the context of this formalism we can study of the details of the interactions in order to compare then with other theoretical models, like Effective String Theory, and get a better understanding of the virtues and limitations of this kind of effective models. It is important to check these predictions in the context of different groups. This result is already well set in $3D$ for $SU(2)$ gauge group and some other groups (like $\mathcal{Z}_2$) and some studies are being conducted in this moment like with $SU(3)$ gauge group. Some studies have been done in $U(1)$ gauge group although its results are not yet completely well established. We decided to study the structure of flux tubes produced by static charges in $U(1)$ Lattice Gauge Theory (LGT) in order to try to give a contribution to settle this subject.

1.1 Lattice Quantum Field Theory

LQFT is a discretized Quantum Field Theory that allows to perform non-perturbative numerical Quantum Field Theory computations, as well as some analytical calculations, including perturbative ones.

LGT was first proposed by Wilson in 1974 [1] as an alternative ultraviolet cutoff method, allowing to perform analytical computations and obtaining continuum limits.

Soon after people started to explore the possibilities that lattice approach opens in direct numerical evaluation of gauge theories. In 1981 Hamber and Parisi publish for the first time a hadronic mass spectrum obtained from lattice QCD in quenched approximation [2], demonstrating in practice the possibility of performing this kind of calculations. With time LGT became regarded as the natural way for calculating numerical non-perturbative quantities.

Progressively people obtained a much deeper understanding of systematical errors and the 2000's, with the development of algorithms and computational power, have seen the appearance of unquenched calculations, with the effects of quark loops being taken into account.

Although in 2001 people feared it would be impossible to reach realistic quark masses, independently of computational power available, due to an enormous rise in the calculation time needed with the algorithms available, the recent development of new algorithms solved this problem and opened the possibility of approaching limits where realist calculations can be performed.

In this moment this calculations are being done and LQFT seems to have a promising role in next years in physics.

1.1.1 Spacetime Discretization

In LQFT we want to build a theory that can evaluate the path integral directly in a computer. As computers cannot deal with a continuous spacetime the first obvious step is to discretize it. There are several possible approaches to this, being that the most widely used is the discretization of space time in an isotropic hypercubic lattice with a certain lattice spacing between points. This spacing can be determined *a posteriori* by the appropriate matching of lattice quantities with physical measured quantities or can just be taken as a parameter which computed quantities depend on.

This isotropic hypercubic lattice is the simplest choice that can be taken and, although other approaches have been tried sporadically , it remains the almost exclusively used discretization. This hypercube will have dimensions $N_S \times N_S \times N_S \times N_T$ and periodical boundary conditions in all directions[1].

The next step consists in introducing the fields in the lattice in a way that they preserve the proprieties we are interested in. This is done by considering the fermions as Grassman variables laying in the lattice sites and the gauge fields as group elements in the links between lattice sites. So we assign the gauge field in the links the average value of the field in between the two nearest points. We will see that this definition allows to preserve gauge invariance.

We denote the fermions by ψ and the gauge field by U_μ.

1.1.2 Gauge invariance

It is important to preserve the gauge symmetry of the original theory. To do so we need to understand how to build gauge invariant quantities in the lattice we just defined. First of all let us transcribe the notion of gauge freedom to the lattice. Gauge freedom is the freedom to perform a local gauge transformation of our fields, which can be expressed as the multiplication of a gauge element locally. In lattice a general gauge transformation can be parametrized as

$$\psi(x) \to V(x)\psi(x) \tag{1}$$
$$\bar{\psi}(x) \to \bar{\psi}(x)V^{-1}(x) \tag{2}$$
$$U_\mu(x) \to V(x)U_\mu(x)V^{-1}(x+\hat{\mu}) \tag{3}$$
$$U_\mu^{-1}(x) \to V(x+\hat{\mu})U_\mu^{-1}(x)V^{-1}(x). \tag{4}$$

In a general way, we have two types of possible gauge invariant quantities on lattice

- the trace of a closed loop $U(x,y;\mathcal{C})$ (a generalization of our plaquette example)

$$\begin{aligned}\mathrm{Tr}\left[U(x,x;\mathcal{C})\right] &\to \mathrm{Tr}\left[U'(x,x;\mathcal{C})\right] = \\ &= \mathrm{Tr}\left[V(x)U(x,x;\mathcal{C})V^{-1}(x)\right] = \\ &= \mathrm{Tr}\left[U(x,x;\mathcal{C})\right]\end{aligned} \tag{5}$$

- a path that starts and ends in an antifermion and a fermion

$$\begin{aligned}\bar{\psi}(x)U(x,y;\mathcal{C})\psi(y) &\to \bar{\psi}'(x)U'(x,y;\mathcal{C})\psi'(y) = \\ &= \bar{\psi}(x)V^{-1}(x)V(x)U(x,y;\mathcal{C})V^{-1}(y)V(y)\psi(y) \\ &= \bar{\psi}(x)U(x,y;\mathcal{C})\psi(y).\end{aligned} \tag{6}$$

1.1.3 Action

The action choice is not unique, we can accept several actions since they respect gauge invariance and have the right continuum limit.

The correct limit of the gauge action in continuum should be the well-known Yang-Mills action

$$S_G = -\frac{1}{4}\int \mathrm{d}^4x \ \mathrm{Tr} F_{\mu\nu}F^{\mu\nu}. \tag{7}$$

We can start by taking our example of the plaquette operator we defined before. We will do this in the Abelian case, the case of most interest for us in this dissertation. The non-Abelian case is not very different (although the calculations are somewhat lengthier and more complicated). We have

$$P_{\mu\nu}(x) = U_\mu(x)\ U_\nu(x+\hat{\mu})\ U_\mu^{-1}(x+\hat{\nu})\ U_\nu^{-1}(x) \tag{8}$$

It makes sense to define

$$U_\mu(x) \equiv \mathrm{e}^{iag\left[A_\mu(x+\frac{\hat{\mu}}{2})\right]} \tag{9}$$

[1] Again this choice is not unique. Recently there have been attempts to work with lattices that are not periodic in time [3], which allows to solve some topology related technical problems, although it is not yet well explored.

once the link values are defined in the middle point of the link. This way in the new variables the plaquette will be

$$P_{\mu\nu}(x) = \mathrm{e}^{iag\left[A_\mu(x+\frac{\hat{\mu}}{2})+A_\nu(x+\hat{\mu}+\frac{\hat{\nu}}{2})-A_\mu(x+\hat{\nu}+\frac{\hat{\mu}}{2})-A_\nu(x+\frac{\hat{\nu}}{2})\right]} = \\ = \mathrm{e}^{iag\left[A_\mu(r-\frac{\hat{\nu}}{2})+A_\nu(r+\frac{\hat{\mu}}{2})-A_\mu(r+\frac{\hat{\nu}}{2})-A_\nu(r-\frac{\hat{\mu}}{2})\right]} \tag{10}$$

where r is the coordinate of the center of the plaquette. Noting that $A_\mu(r-\frac{\hat{\nu}}{2}) = A_\mu(r) + \partial_\nu A_\mu\left(-\frac{a}{2}\right) + \mathcal{O}(a^2)$ we have in the exponent

$$iag[A_\mu(r-\frac{\hat{\nu}}{2}) - A_\mu(r+\frac{\hat{\nu}}{2}) + A_\nu(r+\frac{\hat{\mu}}{2}) - A_\nu(r-\frac{\hat{\mu}}{2})] = \\ = iag[A_\mu(r) - \frac{a}{2}\partial_\nu A_\mu - A_\mu(r) - \frac{a}{2}\partial_\nu A_\mu + A_\nu(r) + \frac{a}{2}\partial_\mu A_\nu - \\ - A_\nu(r) + \frac{a}{2}\partial_\mu A_\nu + \mathcal{O}(a^2)] = \\ = iag[\partial_\mu A_\nu - \partial_\nu A_\mu + \mathcal{O}(a^2)] = ia^2 g F_{\mu\nu} + i\mathcal{O}(a^3). \tag{11}$$

Expanding now the exponential we can get

$$P_{\mu\nu}(x) = \mathrm{e}^{ia^2 g F_{\mu\nu} + i\mathcal{O}(a^3)} = \\ = 1 + ia^2 g F_{\mu\nu} - \frac{a^4 g^2}{2} F_{\mu\nu}^2 + i\mathcal{O}(a^3) + \mathcal{O}(a^5). \tag{12}$$

So the real part of plaquette contains the square of the components of the electromagnetic tensor[2]. This way we can take the action to be

$$S_g = \beta \sum_x \sum_{\mu<\nu} \mathrm{Re}\left[1 - P_{\mu\nu}(x)\right] \tag{13}$$

where we adopt the usual convention $\beta = \frac{1}{g^2}$.

It is easy to check that this action has as continuum limit the usual Yang-Mills action

$$S_g = \frac{1}{g^2}\sum_x \sum_{\mu<\nu} \mathrm{Re}\left[1 - P_{\mu\nu}(x)\right] = \frac{a^4}{2}\sum_x \sum_{\mu<\nu} F_{\mu\nu}^2 = \\ = \frac{a^4}{4}\sum_x \sum_{\mu,\nu} F_{\mu\nu}^2 \longrightarrow \frac{1}{4}\int \mathrm{d}^4x \; F_{\mu\nu}F^{\mu\nu}. \tag{14}$$

The trace is not needed since we are working with $U(1)$ gauge theory and $U(1)$ group elements commute. In a more general settlement of non-Abelian theories we would have Tr $\mathrm{Re}\left[1 - P_{\mu\nu}(x)\right]$.

This action is the simplest possible and is known as Wilson action.

1.1.4 Monte Carlo Methods

We discretized spacetime and introduced the fields of the theory in the lattice.Usually people resort on Monte Carlo methods for calculations, in practice introducing a new layer of discretization. The process consists in taking the path integral and discretizing it by taking into account only a finite number of field configurations which are representative of the system in thermal equilibrium.

We start with the partition function

$$\mathcal{Z} = \int \mathcal{D}\phi \; \mathrm{e}^{iS[\phi]}. \tag{15}$$

If we effectuate a Wick rotation, we have

$$\mathcal{Z}_E = \int \mathcal{D}\phi_E \; \mathrm{e}^{-S_E[\phi_E]} \tag{16}$$

and

$$\langle O\rangle_E = \frac{\int \mathcal{D}\phi_E \; O_E[\phi_E] \; \mathrm{e}^{-S_E[\phi_E]}}{\int \mathcal{D}\phi_E \; \mathrm{e}^{-S_E[\phi_E]}}. \tag{17}$$

where the subscript $_E$ indicates euclidean version, which we will use almost always. From now on, for the sake of simplicity, we will drop the $_E$ subscript whenever the situation is not dubious.

This way we have

$$\langle O\rangle = \mathcal{N}\int \mathcal{D}\phi \; O[\phi] \; \mathrm{e}^{-S[\phi]}. \tag{18}$$

Denominating a configuration for $x^{(\alpha)}$, we can approximate the integral in configurations for the following sum in N_{cf} configurations

$$\langle O\rangle \approx \bar{O} \equiv \frac{1}{N_{cf}}\sum_{\alpha=1}^{N_{cf}} O[x^{(\alpha)}] \tag{19}$$

with a correspondent standard deviation

$$\sigma_{\bar{O}} = \sqrt{\mathrm{Var}\left[\frac{1}{N_{cf}}\sum_{\alpha=1}^{N_{cf}} O[x^{(\alpha)}]\right]} = \sqrt{\frac{1}{N_{cf}^2}\mathrm{Var}\left[\sum_{\alpha=1}^{N_{cf}} O[x^{(\alpha)}]\right]} = \tag{20}$$

assuming that the configurations are independent Bienaymé's formula guarantees that we can perform the following step[3]

$$= \sqrt{\frac{1}{N_{cf}^2}\sum_{\alpha=1}^{N_{cf}} \mathrm{Var}\left[O[x^{(\alpha)}]\right]} = \sqrt{\frac{\sigma_O^2}{N_{cf}}} \propto \frac{1}{\sqrt{N_{cf}}}. \tag{21}$$

[2] Although not relevant here it's easy to check that, unlike with non-Abelian theories, in $U(1)$ it is possible to probe the electric field directly using the imaginary part of the plaquette.

[3] Bienaymé's formula is a theorem that states that the variance of the sum of independent random variables is equal to the sum of the variances of those variables. For a proof check for example [4].

1.2 Effective String Theory

Effective string theory is an effective bosonic string theory that is believed to model successfully many aspects of confining theories. This was proposed long ago and was initially supported by two arguments [5]: meson spectroscopy could be explained assuming a string-like interaction between quarks; and the discovery that in strong coupling limit the interquark potential rises linearly.

Many papers were published about this subject and many predictions of effective string theory have been studied. It predicts the formation of a flux tube between charges, giving origin to an asymptotically linear potential, responsible by the confinement property of the theory.

Its most famous result is the shape of the confining potential [6]

$$V(r) = A + \sigma r + \frac{\gamma}{r} + \mathcal{O}(1/r^3) \tag{22}$$

where $\gamma = \frac{(d-2)\pi}{24}$ and d is the dimension of the spacetime. This potential have some striking properties namely being independent of the gauge group we chose for the interaction. Also the numerical value of γ, known as Lüscher term, is a dimensionless constant thought to be independent of gauge group, just depending on the dimensionality of spacetime.

Recently there have been progress in this area with the calculation of the energy spectrum of the theory up to higher orders (e.g. [7]).

Other important results of this theory are the predictions about the width of the flux tube. The theory predicts that the flux tube width should increase logarithmically with the distance between the sources at zero temperature and linearly at high temperature

- zero temperature $w^2_{lo}(r/2) = \frac{d-2}{2\pi\sigma}\log(\frac{r}{r_0})$
- finite temperature $w^2_{lo}(r/2) = \frac{d-2}{2\pi\sigma}\log\frac{N_t}{4r_0} + \frac{d-2}{4N_t\sigma}r + O(\mathrm{e}^{-2\pi r/N_t})$

where N_t is the temporal extent of the lattice, d is the dimension of spacetime and r_0 is some scale to be fitted.

These expressions have been recently shown [8, 9] to be correspondingly the low and high temperature limits of the same expression that incorporates the dependence of temperature explicitly

$$w^2_{lo}(r/2) = \frac{d-2}{2\pi\sigma}\log\left(\frac{r}{\rho_0}\right) + \frac{d-2}{\pi\sigma}\log\left(\frac{\eta(2iu)}{\eta^2(iu)}\right) \tag{23}$$

where η is Dedekind η function and $u = \frac{N_t}{2r}$ incorporates the temperature dependence.

This way the only fit constants are r_0 and σ, and σ can be fixed precisely from independent measurements of the potential at zero temperature.

1.3 CUDA

CUDA (Computer Unified Device Architecture) is a computer architecture developed by NVIDIA that allows to explore the graphics processing units (GPU's) for general purpose calculations. We use CUDA extensions of C++ programming language, which consist a set of extensions for this language that allow to use many features of C++, like classes and templates in GPU calculations.

Due to the challenges faced by graphics processing, GPU architecture have evolved into devices extremely well suited for highly parallelized code execution, with many cores and high memory bandwidth. This is ideal for lattice QCD calculations, because this calculations typically involve the analysis of all points of lattice independently which results in highly parallelizable calculations.

We use NVIDIA Fermi generation GPU's that support double precision operations and allow the necessary performance for our calculations.

For our calculations we resorted mainly to four GPU's, two NVIDIA GeForce GTX 580 and two NVIDIA Tesla C2075.

2 Methods

2.1 Generation of configurations

We want to generated a set of configurations which should be decorrelated of each other (ideally independent), so we can guarantee that our estimate for the error is correct.

We define the autocorrelation of configurations as

$$C(x^{(a)}, x^{(b)}) = \frac{1}{V \times d}\left|\sum_x \sum_\mu \left[U^{(a)}_\mu(x)\right]^{-1} U^{(b)}_\mu(x)\right|. \tag{24}$$

2.2 Errors estimation

We use Jackknife method for error estimation. This method was introduced in 1956 by Quenouille[10] and two years latter by John Tukey[11].

It provides a method for estimating the variance of a general unknown distribution. It consists in systematically taking points out of the average and checking how much does it change, relating this change to the variance of the distribution.

If we have a dataset with N measurements of an observable x with average $\bar{x}$ we define $\bar{x}_j = \frac{1}{N-1}\sum_{i\neq j} x_i$ (the average extracting the measurement j). So for the variance of the average $\bar{x}$ we have the following expression [12]

$$\sigma_x^2 \equiv \frac{N-1}{N}\sum_{i=1}^{N}\left(\bar{x}_j - \bar{x}\right)^2 \tag{25}$$

It can also be generalized to a method in which the data is group in bins of a certain size, where an appropriate choice of bin sizes allows to solve the problems related to the absence of statistical independence between consecutive measurements.

2.3 Metropolis algorithm

Metropolis algorithm is a Monte Carlo algorithm that allows to draw samples from a probability distribution. It produces a Markov chain of lattice configurations when applied sequentially to an initial configuration.

It is a simple algorithm that consists in the following procedure [13]:

- generate a new random link θ_{new} with uniform probability within the group
- if the action of the new link decreases accept it automatically, otherwise accept it with probability $\mathrm{e}^{-S_{new}}/\mathrm{e}^{-S_{old}}$.

2.4 Overrelaxation

In some regions of β pure Metropolis method exhibits a long autocorrelation time between configurations. Because of that the need for a method which decorrelates faster becomes important.

Overrelaxation is a widely used method for this propose. It decorrelates the system faster without changing the value of the action (so it changes a configuration to a different one which has equal probability of occurrence).

The one we implement corresponds in practice to a reflection of the value of the links in relation to the minimum action so

$$\mathrm{e}^{i\theta} \to \mathrm{e}^{i(\theta_{min}+(\theta_{min}-\theta))} = \mathrm{e}^{i(2\theta_{min}-\theta)} \tag{26}$$

where θ_{min} is to the phase that would minimize the action given fixed links around it. As Wilson action is symmetric for reflections about its minimum this change keeps the action constant. We implement this by applying overrelaxation to a direction at a time keeping the others constant.

This method decorrelates configurations much faster than using metropolis method alone.

2.5 Multihit

A technique frequently applied to reduce the statistical error is multihit. It consists in a replacement of the links in time direction with effective links calculated through an average process against a constant background.

This new variables have the same average of the old links but a smaller variance so they have smaller statistical errors than the traditional links. Most of the times this average is evaluated stochastically, but in $U(1)$, as we will see, this substitution can be easily done analytically. This analytical process is frequently referred to as link integration.

The procedure corresponds to the following substitution [14, 15]

$$U_\mu(x) \to \frac{\int \mathrm{d}U\, U\exp(-\beta S)}{\int \mathrm{d}U\exp(-\beta S)} = \frac{I_1(\beta|W_\mu(x)|)}{I_0(\beta|W_\mu(x)|)}\frac{W_\mu(x)}{|W_\mu(x)|} \tag{27}$$

where I_0 and I_1 are the modified Bessel functions of order 0 and 1 and $W_\mu(x)$ is the sum of the staples of the $U_\mu(x)$ link. If calculating correlations between links in the same temporal layer, they should be spaced of at least two lattice spacings to ensure the result is correct.

2.6 Lüscher-Weisz Multilevel

Multilevel algorithm was purposed by Martin Lüscher and Peter Weisz in 2001[16] as a method for achieving exponential error reduction in some LGT calculations. It is useful when the lattice is in confining phase and a local action is used, especially for evaluating average values of Polyakov or Wilson loops.

2.6.1 Method

This method is inspired on the multihit method and explores the locality of the action by factorizing the path integral into smaller integrals calculated over sublattices.

We will start by introducing two-link operators since they play an essential in the formulation of the theory. Two-link operators are structures defined from the tensor product of two links in the same time layer at a certain distance r. This structure represents the propagation in time of a pair of fermions from time t to time $t+1$ and they can be regarded as the basic constituents of the Polyakov loop correlation or of the temporal part of Wilson loop. They are defined as the following

$$\mathbb{T}(x,t,r,\mu) = U_0^*(x+t\hat{0})\; U_0(x+t\hat{0}+r\hat{\mu}). \tag{28}$$

We can note that this structure would be much more complicated in non-Abelian theories, since although in $U(1)$ the tensor product reduces to the usual product of two complex numbers this is not the case in general.

Now we can rewrite the Polyakov loop correlation in terms of these newly defined variables

$$\begin{aligned} P(x)^* P(x+r\hat{\mu}) = \ & (U_0(x)...U_0(x+T\hat{0}))^* (U_0(x+r\hat{\mu})... \\ & ...U_0(x+T\hat{0}+r\hat{\mu})) = \\ & = \mathbb{T}(x,0,r,\mu)...\mathbb{T}(x,t,r,\mu)...\mathbb{T}(x,T,r,\mu). \end{aligned} \tag{29}$$

Next we will see how we can break the Polyakov loop correlation written like this in a product of averages over sublattices.

To do so we need to find a way of isolating sublattices from within our lattice. These sublattices are time-slices of our original lattice, contained between two hyperplanes of constant time x_0 and y_0. If we take two of those hyperplanes and hold their spatial links constant we can isolate the dynamics of the sublattice from the rest. This can be done thanks to the locality of the action (because the action only depends on plaquettes adjacent to it). This way we can calculate subaverages of quantities inside the smaller lattice. We follow the usual convention and denote the sublattice expectation values with square brackets [...] and expectation values over the whole lattice as $\langle ... \rangle$.

It is now possible to separate the integral in a hierarchical integration process with several intermediate levels. This integrals satisfy identities like $[\mathbb{T}(x,t)\mathbb{T}(x,t+1)] = [[\mathbb{T}(x,t)][\mathbb{T}(x,t+1)]]$, so for example we can calculate the average of the Polyakov loop correlation like this

$$\begin{aligned} \langle P^* P \rangle = \langle & [[\mathbb{T}(x,t)][\mathbb{T}(x,t+1)]][[\mathbb{T}(x,t+2)][\mathbb{T}(x,t+3)]]... \\ & ...[[\mathbb{T}(x,N_t-2)][\mathbb{T}(x,N_t-1)]]\rangle. \end{aligned} \tag{30}$$

It is easy to check that the innermost average corresponds to a multihit process because it fixes the spatial links everywhere and averages the link. This way the multilevel algorithm can be seen as a generalization of multihit.

2.6.2 Polyakov loop correlation

For calculating Polyakov loop correlation is useful to introduce some auxiliary quantities that will be averaged in the sublattices.

Here we follow approximately the notation defined in [15]. We start by defining the operator

$$\mathbb{T}^{(2)}(x,t,r,\mu) = \mathbb{T}(x,t,r,\mu)\mathbb{T}(x,t+1,r,\mu). \tag{31}$$

If we define the first average as an average in sublattices of thickness 2 we have Polyakov loop correlation

$$\begin{aligned} \langle P^* P \rangle = \langle & [\mathbb{T}^{(2)}(x,0,r,\mu)][\mathbb{T}^{(2)}(x,2,r,\mu)]... \\ & ...[\mathbb{T}^{(2)}(x,N_t-2,r,\mu)]\rangle. \end{aligned} \tag{32}$$

In our code we implemented one more level in order to achieve a further reduction on errors, calculating

$$\begin{aligned} \langle P^* P \rangle = \langle & [[\mathbb{T}^{(2)}(x,0,r,\mu)][\mathbb{T}^{(2)}(x,2,r,\mu)]]... \\ & ...[[\mathbb{T}^{(2)}(x,N_t-4,r,\mu)][\mathbb{T}^{(2)}(x,N_t-2,r,\mu)]]\rangle. \end{aligned} \tag{33}$$

In practice the algorithm proceeds in a nested scheme as illustrated in figure 1.

2.6.3 Electromagnetic Field

In section 1.1 we saw how to expand the plaquette

$$P_{\mu\nu} = 1 + ia^2 g F_{\mu\nu} - \frac{a^4 g^2}{2} F_{\mu\nu}^2 + i\mathcal{O}(a^3) + \mathcal{O}(a^5). \tag{34}$$

So we can measure electromagnetic field tensor components through the study of the imaginary part of the plaquette operator

$$\mathrm{Im} P_{\mu\nu} = a^2 g F_{\mu\nu} + \mathcal{O}(a^3). \tag{35}$$

Since $g = 1/\sqrt{\beta}$ we have

$$a^2 F_{\mu\nu} = \sqrt{\beta}\ \mathrm{Im} P_{\mu\nu} + \mathcal{O}(a^3). \tag{36}$$

Similarly if we want to study the squared electromagnetic field we can take the real part of the plaquette

$$a^4 F_{\mu\nu}^2 = 2\beta\ (1 - \mathrm{Re} P_{\mu\nu}) + \mathcal{O}(a^6). \tag{37}$$

We want to study the field produced by static charges at a certain distance of each other so we should correlate our operator with a Polyakov loop correlation representing those charges, getting

$$\langle O \rangle_{P^* P} = \frac{\langle P^* P O \rangle}{\langle P^* P \rangle} - \langle O \rangle \tag{38}$$

where O stands for any operator we want to measure and $\langle O \rangle_{P^* P}$ stands for the expectation value of O produced by the charges represented by $P^* P$.

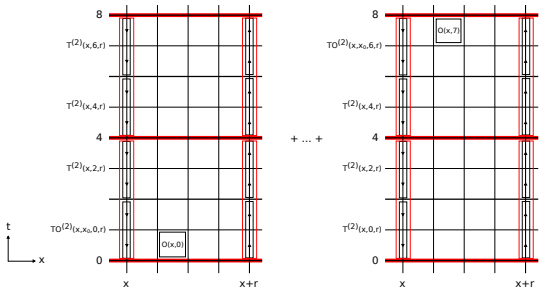

Figure 2: Multilevel method for electromagnetic field.

Repeat level 0 process n_0 times; average the results ($\langle P^*P\rangle$)

Level 0

Update the whole lattice k_0 times
Repeat level 4 process n_4 times; average the results ($[[\mathbb{T}^{(2)}][\mathbb{T}^{(2)}]]$)

Level 4

Update the lattice k_4 times freezing spacial links in layers with t multiple of 4
Repeat level 2 process n_2 times; average the results ($[\mathbb{T}^{(2)}]$)

Level 2

Update the lattice k_2 times freezing spacial links in layers with t multiple of 2
Calculate $\mathbb{T}^{(2)}$

Calculate $[\mathbb{T}^{(2)}][\mathbb{T}^{(2)}]$

Calculate P^*P

Figure 1: Multilevel algorithm.

To implement a multilevel algorithm for this calculation it is useful to introduce some more quantities, besides $\mathbb{T}$ and $\mathbb{T}^{(2)}$,

$$\mathbb{TO}^{(2)}(x_0,x,t,r,\mu) = [\mathbb{T}(x,t,r,\mu)\mathbb{T}(x,t+1,r,\mu)O(x_0,t)+ + \mathbb{T}(x,t,r,\mu)\mathbb{T}(x,t+1,r,\mu)O(x_0,t+1)] \quad (39)$$

$$\mathbb{T}^{(4)}(x,t,r,\mu) = [\mathbb{T}^{(2)}(x,t,r,\mu)][\mathbb{T}^{(2)}(x,t+2,r,\mu)] \quad (40)$$

$$\mathbb{TO}^{(4)}(x_0,x,t,r,\mu) = =[\mathbb{T}^{(2)}(x,t,r,\mu)][\mathbb{TO}^{(2)}(x_0,x,t+1,r,\mu)]+ +[\mathbb{TO}^{(2)}(x_0,x,t,r,\mu)][\mathbb{T}^{(2)}(x,t+1,r,\mu)]. \quad (41)$$

With this notation we can write

$$\langle P^*(0)P(r\hat{\mu})O(x_0)\rangle = \frac{1}{N_S^d N_t d}\sum_x\sum_\mu[[\,\mathbb{TO}^{(4)}(x_0,x,0,r,\mu)\mathbb{T}^{(4)}(x,4,r,\mu)...\mathbb{T}^{(4)}(x,N_t-4,r,\mu) + + \mathbb{T}^{(4)}(x,0,r,\mu)\mathbb{TO}^{(4)}(x_0,x,4,r,\mu)...\mathbb{T}^{(4)}(x,N_t-4,r,\mu)+... ... + \mathbb{T}^{(4)}(x,0,r,\mu)\mathbb{T}^{(4)}(x,4,r,\mu)...\mathbb{TO}^{(4)}(x_0,x,N_t-4,r,\mu)] \quad (42)$$

which can be calculated in a way analog to the Polyakov loop correlation.

3 Results

3.1 Average plaquette density

Average plaquette density is known to have a phase transition, known as bulk transition, which corresponds to a transition in the lattice spacing a.

This phase transition can be clearly observed as a peak in plaquette susceptibility ($\langle P_\mu^2\rangle - \langle P_\mu\rangle^2$) (cf. figure 3).

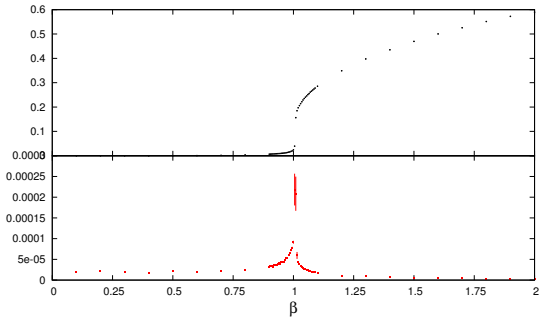

Figure 3: On top polyakov expectation value, on bottom plaquette susceptibility in a lattice of size 8^4.

We study $1-\langle P_{\mu\nu}\rangle$ which is the quantity most often studied in literature instead of $\langle P_{\mu\nu}\rangle$ (cf. figure 4).

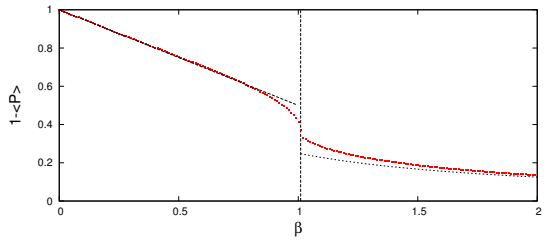

Figure 4: Average plaquette density in function of β. The error bars are much smaller than the size of the points in the graph. The functions plotted are the strong and the weak coupling limits calculated for the theory. The vertical line corresponds to β_c extracted from Polyakov loop expectation value.

Our results for plaquette reproduce closely the results that can be found in many publications.

3.2 Confining phase transition

Confining/deconfining transition can be studied through the analysis of different parameters. The best parameter to study this is Polyakov loop expectation value. Polyakov loop expectation value is 0 in confining phase and rises fast after the phase transition, making it possible to use it as an order parameter for this phase transition (cf. figure 3).

3.3 Multilevel convergence

The multilevel parameters should be tuned to obtain better results. The number of necessary iterates grows exponentially with the interquark distance [16], in order to compensate the exponential growing of the relative error in Polyakov correlations (due to exponential decay of Polyakov correlations). To illustrate this we show the behavior of Polyakov loop correlation with the number of multilevel iterates for different distances (figure 5). It is clear from the figure that the Polyakov loop correlations fall exponential with the distance as well as that the number of multilevel iterates to obtain a stable results grow in an approximately exponential way too.

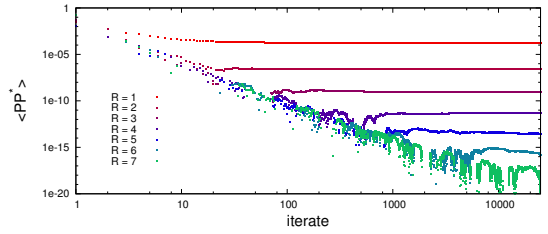

Figure 5: Polyakov loop correlation convergence with multilevel iterate.

3.4 Potential

Static potential can be obtained through the study of Polyakov loop since we have

$$\langle P^*(0)P(r)\rangle = \mathrm{e}^{-N_t V(r)}. \tag{43}$$

This way we have

$$V(r) = -\frac{1}{N_t}\ln\left[\langle P^*(0)P(r)\rangle\right]. \tag{44}$$

We computed the static charge potential with several values of β with and without multilevel. For the confining phase we obtain values compatible with the potential described by effective string theory, for the non-confining phase we obtain an $1/r$ dipole potential.

For $\beta = 1.00$, in the confining phase, we calculate the potential from 100 multilevel configurations, each one with 100 level 4 and 1000 level 2 multilevel iterates, with multihit method for further error reduction (except for $r/a = 1$). We fit the results (figure 6) and extract a value for string tension of $\sigma = 0.16719 \pm 0.00030$, if we force the Lüscher term to be constant ($\chi^2/dof = 0.140$). With Lüscher term as a fit parameter we obtain $\sigma = 0.1666 \pm 0.0022$ and Lüscher term 0.274 ± 0.061 ($\chi^2/dof = 0.147$), in a good agreement with the expected value of $\pi/12 = 0.2618$. We do not include the first two points in the fit.

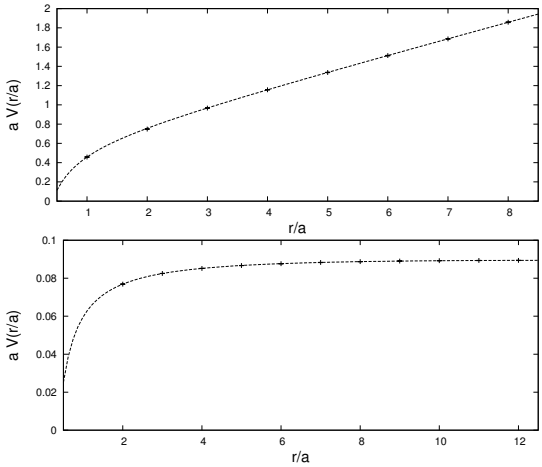

Figure 6: Potential of two static charges at $\beta = 1$ (top) and $\beta = 3$ (bottom). The error bars are much smaller than the size of the points in the graph.

For $\beta = 3.00$, now in the non-confining phase, we can observe the string tension going to zero. Multilevel is not needed in this region since the results are numerically much more stable. We use 1000 configurations, 10 iterates away from each other, and obtain the results in figure 6. From the fit we extract the values of $\sigma = -0.000194 \pm 0.000019$ and for the coefficient of the term in $1/r$ 0.03468 ± 0.00062 ($\chi^2/dof = 0.526$).

From the potential fits we can extract the value of the string tension σ in function of β (cf. figure 7). We can observe the string tension going to zero at deconfining phase transition. We extract also the value of Lüscher term which is compatible with the expected value in the confining phase of $\pi/12$ (cf. figure 8).

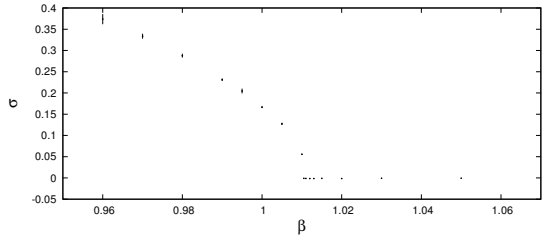

Figure 7: Dependence of string tension with β.

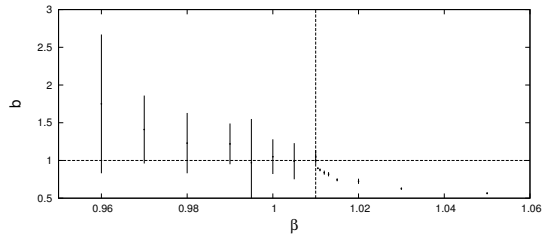

Figure 8: Dependence of $1/r$ term with β (normalized to $\pi/12$).

3.5 Flux tube profile

We calculated the E_x tube profile in the middle plan between the charges using 100 multilevel configurations[4].

To the result we fit the ansatz suggested in [18]

$$\frac{\langle P^* P\ F_{\mu\nu}\rangle}{\langle P^* P\rangle} = A\exp(-x_\perp^2/s)\frac{1+B\exp(-x_\perp^2/s)}{1+D\exp(-x_\perp^2/s)}. \quad (45)$$

As expected we can notice that the flux tube (figure 9) gets broader at bigger charge separations. In the next section (3.6), we quantify this result through the calculation of the flux tube width.

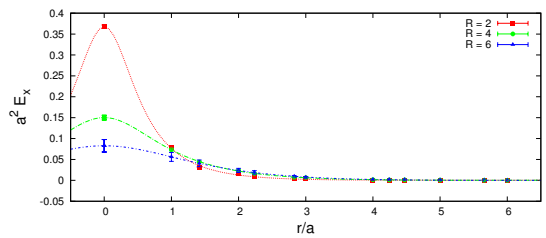

Figure 9: Flux tube profile for several charge distances at $\beta = 1.00$.

3.6 Flux tube width

We integrate $\langle E^2 + B^2\rangle$ ansatz fits to calculate the flux tube width (cf. table 10). The errors are estimated using a jackknife algorithm.

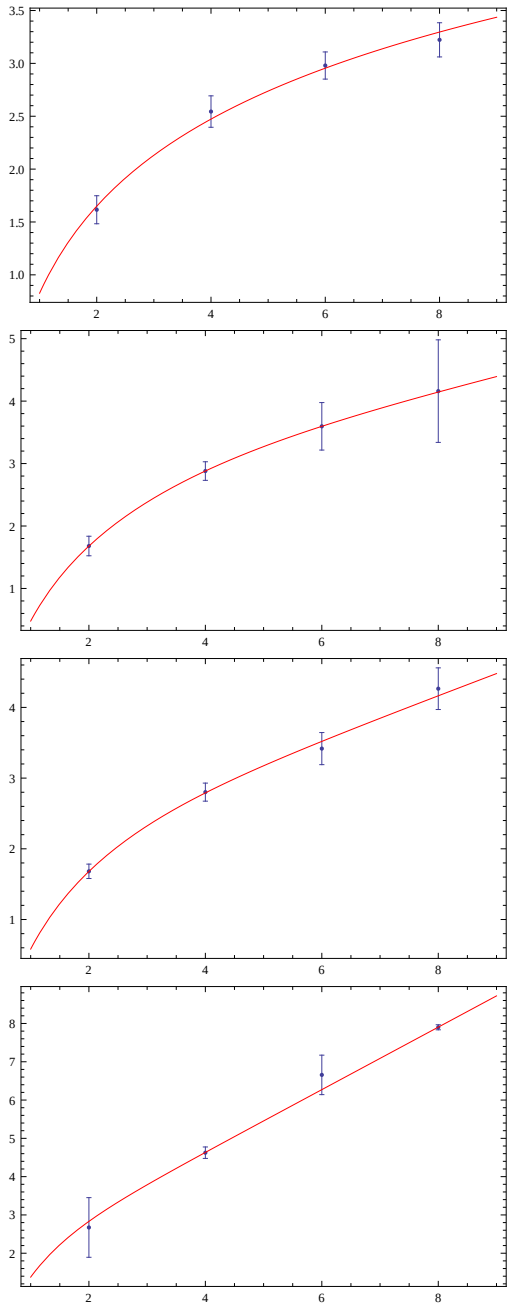

Figure 10: Squared width in function of charge separation for 24 (a), 12 (b), 8 (c) and 4 (d). The figures are plots of $a^2w^2(r/a)$ vs r/a.

[4]These results were presented at Excited QCD 2012 International Meeting. For the corresponding proceeding check [17]. About the width of the flux tube the results we present are an improvement over the ones since now we went to $r/a = 8$, instead of just 6, and we calculated the flux tube width using $\langle E^2 + B^2\rangle$, instead of the $\langle E_x^2\rangle$ presented at the conference.

4 Conclusion

In this work we successfully implemented a gpu code to generate and study $U(1)$ field configurations. We applied it to the study of $U(1)$ flux tubes in confining phase, as well as some other already well-known quantities.

Our results for potential are in a good agreement with the predictions of the effective string model in the confining phase, not only showing an asymptotically linear potential, but also being compatible with a Lüscher term of $\pi/12$.

In the non-confining phase the results follow the expected Coulomb $1/r$ potential, with the string tension going fast to zero.

We study flux tubes in the range from 0.05 T_c to 0.4 T_c and find the results to be in agreement with the predictions of effective string theory. There is a discrepancy between string tension calculated through potential and string width it would be interesting to verify if we can account for it using a higher order result for the theoretical prediction. In a study with $SU(2)$ group in 3D (cf. [18]) going further than leading order is important to account for the correct result at small distances. We calculated the flux tubes up to $r/a = 8$ that to our knowledge is the longest distance obtained up to now without duality transformations. Also the lattice size used in this work (24^4) is bigger than most of the lattice sizes used in literature in $U(1)$ studies (typically $\leq 16^4$). Further research is needed, to increase the precision of the result with more configurations and to obtain more points to the fit, possibly by calculating the r/a odd points and using different β values.

References

[1] K. G. Wilson, "Confinement of quarks," *Phys. Rev. D* **10** (Oct, 1974) 2445–2459. http://link.aps.org/doi/10.1103/PhysRevD.10.2445.

[2] H. Hamber and G. Parisi, "Numerical Estimates of Hadronic Masses in a Pure SU(3) Gauge Theory," *Phys.Rev.Lett.* **47** (1981) 1792.

[3] M. Luscher and S. Schaefer, "Lattice QCD without topology barriers," *JHEP* **1107** (2011) 036, arXiv:1105.4749 [hep-lat].

[4] M. Loève, *Probability Theory*. No. v. 1 in Graduate Texts in Mathematics. Springer-Verlag, 1978.

[5] M. Caselle, R. Fiore, F. Gliozzi, M. Hasenbusch, and P. Provero, "String effects in the Wilson loop: A High precision numerical test," *Nucl.Phys.* **B486** (1997) 245–260, arXiv:hep-lat/9609041 [hep-lat].

[6] M. Luscher, "Symmetry Breaking Aspects of the Roughening Transition in Gauge Theories," *Nucl.Phys.* **B180** (1981) 317.

[7] M. Luscher and P. Weisz, "String excitation energies in SU(N) gauge theories beyond the free-string approximation," *JHEP* **0407** (2004) 014, arXiv:hep-th/0406205 [hep-th].

[8] F. Gliozzi, M. Pepe, and U.-J. Wiese, "The Width of the Color Flux Tube at 2-Loop Order," *JHEP* **1011** (2010) 053, arXiv:1006.2252 [hep-lat].

[9] F. Gliozzi, M. Pepe, and U.-J. Wiese, "The Width of the Confining String in Yang-Mills Theory," *Phys.Rev.Lett.* **104** (2010) 232001, arXiv:1002.4888 [hep-lat].

[10] M. H. Quenouille, "Notes on bias in estimation," *Biometrika* **43** no. 3-4, (1956) 353–360, http://biomet.oxfordjournals.org/content/43/3-4/353.f

[11] J. W. Tukey, "Bias and confidence in not-quite large samples," *The Annals of Mathematical Statistics* **29** no. 2, (1958) 614.

[12] R. G. Miller, "The jackknife-a review," *Biometrika* **61** no. 1, (1974) 1–15, http://biomet.oxfordjournals.org/content/61/1/1.full.

[13] M. Creutz, *Quarks, Gluons and Lattices*. Cambridge Monographs on Mathematical Physics. Cambridge University Press, 1985.

[14] G. Parisi, R. Petronzio, and F. Rapuano, "A Measurement of the String Tension Near the Continuum Limit," *Phys.Lett.* **B128** (1983) 418.

[15] Y. Koma, M. Koma, and P. Majumdar, "Static potential, force, and flux tube profile in 4-D compact U(1) lattice gauge theory with the multilevel algorithm," *Nucl.Phys.* **B692** (2004) 209–231, arXiv:hep-lat/0311016 [hep-lat].

[16] M. Luscher and P. Weisz, "Locality and exponential error reduction in numerical lattice gauge theory," *JHEP* **0109** (2001) 010, arXiv:hep-lat/0108014 [hep-lat].

[17] A. Amado, N. Cardoso, M. Cardoso, and P. Bicudo, "Study of compact U(1) flux tubes in 3+1 dimensions in lattice gauge theory using GPU's," *Acta Physica Polonica B Proceedings Supplement Vol. 5 No 4* (2012) 1129–1134, arXiv:1208.0166 [hep-lat].

[18] F. Gliozzi, M. Pepe, and U.-J. Wiese, "Linear Broadening of the Confining String in Yang-Mills Theory at Low Temperature," *JHEP* **1101** (2011) 057, arXiv:1010.1373 [hep-lat].